

## Colloidal microstructures, transport, and impedance properties within interfacial microelectrodes

Pradipkumar Bahukudumbi, W. Neil Everett, and Ali Beskok

*Department of Mechanical Engineering, Texas A&M University, College Station, Texas 77843*

Michael A. Bevan<sup>a)</sup>

*Department of Chemical Engineering, Texas A&M University, College Station, Texas 77843*

Gregory H. Huff

*Department of Electrical Engineering, Texas A&M University, College Station, Texas 77843*

Dimitris Lagoudas and Zoubeida Ounaies

*Department of Aerospace Engineering, Texas A&M University, College Station, Texas 77843*

(Received 19 March 2007; accepted 7 May 2007; published online 30 May 2007)

The authors report *in situ* measurements of the reversible, electric field mediated assembly of colloidal gold microstructures and their associated impedance properties on surfaces between planar gold film microelectrodes. Video optical microscopy is used to monitor the assembly of wires and locally concentrated configurations having variable resistances and capacitances. A scaling analysis of dominant electrokinetic transport mechanisms at different electric field amplitudes and frequencies is consistent with the observed steady-state microstructures. Impedance spectra are fit to equivalent circuits with elements directly connected to physical characteristics of the microelectronic/fluidic device components and different particle microstructures. © 2007 American Institute of Physics. [DOI: 10.1063/1.2744480]

Numerous studies have investigated colloidal dispersions in electric fields as a means to characterize particle size and surface charge,<sup>1</sup> create electrorheological fluids,<sup>2</sup> separate biocolloids<sup>3</sup> and carbon nanotubes,<sup>4</sup> control display devices,<sup>5</sup> understand fundamental phase behavior,<sup>6</sup> and assemble irreversible nanowires.<sup>7</sup> Such studies are often restricted to a range of applied field voltages and frequencies dictated by the dominance of a particular transport mechanism (e.g., electrophoresis, dielectrophoresis) in a specific application. A comprehensive description of the connections between colloidal microstructural transitions, transport mechanisms, and ac electrical properties is lacking, particularly in the case of interfacial and confined geometries important to integrated microfluidic/electronic devices.

In this letter, we employ *in situ* optical microscopy and impedance measurements to systematically measure microstructures and ac electrical properties of metal colloids in coplanar gold film electrode devices over a broad range of electric field amplitudes and frequencies. This allows us to demonstrate control of impedance characteristics in a microfluidic/electronic device via electric field mediated assembly of various colloidal microstructures. The reversible, fluid nature of such colloidal based devices is shown to exhibit unique impedance responses and tunability not easily achieved with solid-state materials or microelectromechanical devices.

The experimental arrangement consists of nominal 800 nm diameter gold colloids (Alfa Aesar) electrostatically levitated above lithographically patterned gold film electrodes on glass microscope slides. The gold electrodes are 50 nm thick with an interdigitated configuration with 30  $\mu\text{m}$  lateral spacing. Gold colloids were dispersed in aqueous

0.1 mM  $\text{NaHCO}_3$  (conductivity of 9  $\mu\text{S}/\text{cm}$ ) and measured to have a zeta potential of  $-48$  mV (Brookhaven ZetaPALS). The gold colloids are confined within a thin, quasi-two-dimensional (quasi-2D) layer near the surface due to gravity and particle-surface electrostatic repulsion to produce an area fraction of 0.14 within a polydimethylsiloxane batch cell (1 mm high  $\times$  5 mm inside diameter). A function generator (Agilent 33120A) and impedance analyzer (Hewlett-Packard HP4194A) were connected in series to the patterned electrodes to tune colloidal assembly and acquire impedance spectra. An inverted optical microscope (Zeiss) with a 40 $\times$  objective and a charge coupled device camera (Hamamatsu) were used to image steady-state colloidal configurations for the different field conditions shown in Fig. 1.

In the absence of any applied fields, the gold colloids are randomly distributed parallel to the glass and electrode surfaces. In the presence of ac electric fields, Fig. 1 shows a matrix of steady-state microstructures assembled in between and above a single electrode pair gap as a function of ac voltage (0.5–2.5 V) and frequency (10 Hz–1 MHz). All colloidal microstructures in Fig. 1 were reversibly assembled as the result of electrostatic repulsion operating over  $\sim 100$  nm (Debye length is  $\kappa^{-1} = 30$  nm) between colloids and surfaces to prevent strong van der Waals and dipolar adhesion.<sup>2</sup>

The results in Fig. 1 can be organized based on three distinct steady-state microstructures that emerge based primarily on ac field frequency regimes and to a lesser extent on ac field amplitude. For  $\omega \approx 1$ –100 Hz, colloids track the ac field and centrally oscillate within a band in the electrode gap, whereas colloids above the electrodes experience lateral aggregation. For  $\omega \approx 1$ –100 kHz, colloids are expelled from the electrode gap and concentrate on top of the electrodes with a depleted zone near the electrode edges. For  $\omega > 100$  kHz, colloids assemble into chains bridging the elec-

<sup>a)</sup> Author to whom correspondence should be addressed; electronic mail: mabevan@tamu.edu

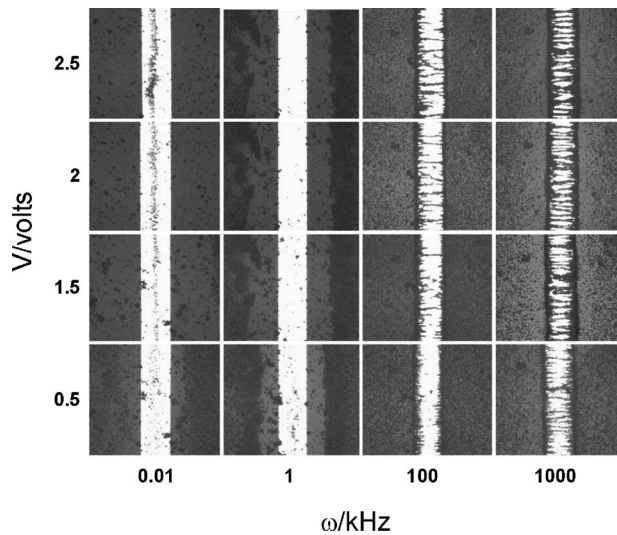


FIG. 1. Optical microscopy images of steady-state configurations of 800 nm gold colloids within a 30  $\mu\text{m}$  gap between interdigitated coplanar gold film electrodes as a function of applied ac electric field frequency and amplitude.

trodes and align with the expected field lines in the gap. For all cases in Fig. 1, greater ac field amplitudes in each frequency regime do not appreciably alter the microstructure type but primarily enhance the assembly rate and the structural fidelity.

The observed structures in Fig. 1 and their transient assembly can be explained in terms of a competition between sedimentation, self-diffusion, and several ac electric field mediated transport mechanisms including electrophoresis (EP), ac electro-osmosis (EO), and dielectrophoresis (DP).<sup>8</sup> In all cases, sedimentation concentrates particles onto the interdigitated electrode surface, and Brownian motion tends to produce laterally homogeneous, random configurations.

To understand the relative transport rates leading to the microstructures in Fig. 1, the dominant single-particle transport mechanisms as a function of ac field amplitude and

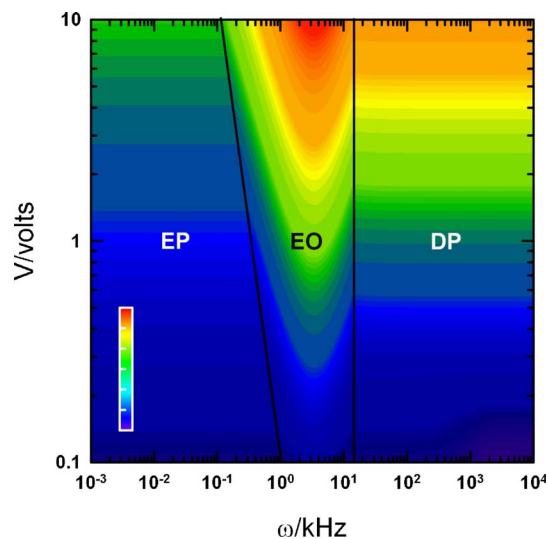


FIG. 2. (Color online) Voltage vs frequency diagram indicating magnitudes of dominant transport mechanisms for single colloids in the coplanar electrode device shown in Fig. 1. Transport rates are computed using Eqs. (1)–(3) and abbreviated as electrophoresis (EP), ac electro-osmosis (EO), and dielectrophoresis (DP). Velocity contours are defined by the logarithmic spectrum scale shown in the inset with red=2000  $\mu\text{m/s}$  and violet=0.01  $\mu\text{m/s}$ .

frequency are reported in Fig. 2. The maximum velocity associated with dynamic EP,  $u_{\text{EP}}$ , for colloids with thin electrical double layers ( $\kappa a \gg 1$ ) is given by<sup>9</sup>

$$u_{\text{EP}} = (\alpha \varepsilon \zeta / \pi \mu m r) [(\alpha / m)^2 + \omega^2]^{-0.5} V, \quad (1)$$

where the quantity  $(\varepsilon \zeta / \mu)(V / \pi r)$  is the Smoluchowski EP rate,<sup>10</sup>  $\varepsilon$  is the medium permittivity,  $\zeta$  is the zeta potential,  $r$  is the electrode gap,  $V$  is the applied voltage (approximately related to the electric field  $E$  for the coplanar geometry as  $E = V / \pi r$ ),<sup>8</sup>  $\alpha = 6 \pi \mu a$  is the Stokes resistance coefficient,  $\omega$  is the frequency,  $m = \rho_c (4/3) \pi a^3$  is the colloid mass, and  $\rho_c$  is the colloid density. ac EO flows due to tangential electric fields determine the transport rate of entrained particles as<sup>8</sup>

$$u_{\text{EO}} = (\Lambda \varepsilon / 8 \mu r) \Omega^2 (1 + \Omega^2)^{-2} V^2, \quad (2)$$

where  $\Lambda = C_S / (C_S + C_D)$ ,  $C_S$  is the Stern layer capacitance,  $C_D$  is the diffuse layer capacitance,  $\Omega = (\Lambda \omega \varepsilon \kappa \pi r / 2 \sigma)$ , and  $\sigma$  is the medium conductivity ( $\Lambda \approx 0.2$  for gold film electrodes with  $C_D = \varepsilon \kappa$  and  $C_S = 0.007 \text{ F/m}^2$ , as discussed in Ref. 8) The rate of colloidal transport and assembly into wires via DP in nonuniform electric fields can be collectively characterized using<sup>11</sup>

$$u_{\text{DP}} = (\varepsilon a^2 / \pi \alpha r^2) f_\phi f_{\text{CM}}^2 \Omega^2 (1 + \Omega^2)^{-1} V^2, \quad (3)$$

where  $f_{\text{CM}} = \text{Re}[(\tilde{\varepsilon}_p - \tilde{\varepsilon}) / (\tilde{\varepsilon}_p + 2\tilde{\varepsilon})]$  is the real part of the Clausius-Mossotti factor ( $f_{\text{CM}} = 1$  for gold colloids),  $\tilde{\varepsilon}$  is the complex permittivity given as  $\tilde{\varepsilon} = \varepsilon - i\sigma/\omega$  (subscript  $p$  refers to particle), and  $f_\phi$  is a correction factor accounting for interparticle spacing, chain orientation, and effective medium dielectric properties at finite colloid concentrations ( $f_\phi \approx 10$  from Ref. 11).

The three dominant transport regimes that emerge in Fig. 2 correlate with the three microstructural regimes observed in Fig. 1, which allows for direct connections to be made between assembly mechanisms and structures. For  $\omega \approx 1$ –100 Hz, EP produces oscillatory colloidal motion within the quasi-2D plane parallel to the substrate (Fig. 1, column 1), although the colloidal localization within a centralized band is probably due to the finite role of recirculating EO flows in producing stagnation regions in between and on top of the electrodes. For  $100 \text{ Hz} < \omega < 100 \text{ kHz}$ , ac EO produces three-dimensional periodic, recirculating flows on the parallel interdigitated electrodes within the confined microfluidic geometry,<sup>12</sup> which is particularly visible during assembly transients. These EO flows eject colloids from the electrode gaps and in combination with sedimentation reconcentrate colloids in stagnation regions on top of the electrodes (Fig. 1, column 2).

The appearance of linear wire structures for  $\omega > 100 \text{ kHz}$  (Fig. 1, columns 3 and 4) occurs as a result of ac electric fields inducing dipoles in colloids, transporting colloids via DP, and assembling colloidal chains via dipolar interactions. Because DP transport occurs within the quasi-2D plane parallel to the substrate and orthogonal to gravity, sedimentation does not compete with dipolar chain assembly, although it may have some influence on confining heavier chains near the surface. As the applied voltage is increased, there is an increase in the number of chains, their rate of formation, and chain “bundling” via lateral dipolar chain attraction.<sup>2</sup>

By understanding ac field mediated microstructure types and dominant transport mechanisms in Figs. 1 and 2, it is

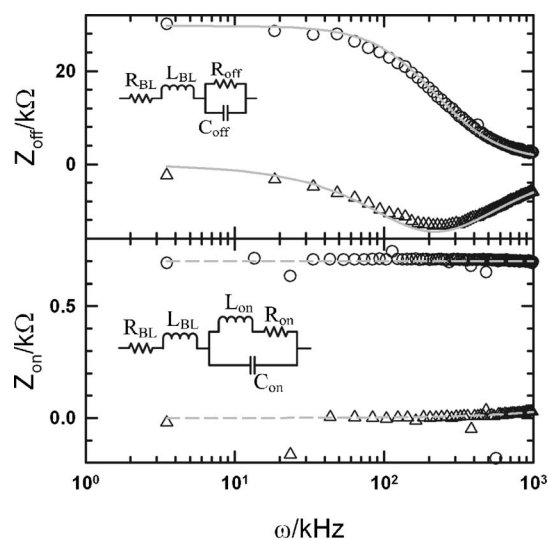


FIG. 3. Measured real (circles) and imaginary (triangles) impedance spectra for (top) no applied field and (bottom) an applied field of 2.5 V and 1 MHz corresponding to the colloidal configuration shown in the upper right corner of Fig. 1. Curve fits to the measured impedance spectra are based on equivalent circuits shown as insets in each case.

possible to interpret the measured impedance spectra in Fig. 3 for colloids in the presence (2.5 V, 1 MHz) and absence (0 V) of applied ac electric fields. As shown in the insets of Fig. 3, equivalent circuits were used to model the measured impedance spectra. Systematic control measurements were used to independently determine the contributions of the substrate, electrodes, electrolyte solution, measurement system, function generator, and different colloidal configurations so that no adjustable parameters were required to specify equivalent circuit components. In both cases in Fig. 3, impedance spectra were reproduced at least five times and accurately modeled by equivalent circuits ( $R^2 > 0.99$ ).

In control measurements, the micropatterned gold film electrodes in air and a current limiting resistor had a combined resistance of  $R_{BL} = 700 \Omega$ , the connecting wires had an inductance of  $L_{BL} = 4.69 \mu\text{H}$ , and the electrolyte media/unassembled colloids had a resistance of  $R_{off} = 29 \text{ k}\Omega$ . The collective capacitance of the electrodes, aqueous media, and gold colloids with and without ac fields was  $C_{on} = C_{off} = 25 \text{ pF}$ . Without the application of an ac electric field, the corresponding impedance spectrum in Fig. 3 is dominated by the properties of the static gold microelectrode arrangement, glass substrate, and aqueous electrolyte media.

In the presence of an applied ac electric field (2.5 V, 1 MHz), the equivalent circuit components representing the device and aqueous media remain unchanged, but the assembled dipolar chains and electrolyte now produce a gap resistance of  $R_{on} = 1.7 \Omega$  and an inductance of  $L_{on} = 17 \text{ fH}$ . With  $\sim 20$  parallel wires/100  $\mu\text{m}$  (from Fig. 1 image) and a 5 mm electrode interface, the resistance per wire is estimated to be 1.7  $\text{k}\Omega$  (resistance per wire length is  $1.7 \text{ k}\Omega/30 \mu\text{m} \approx 60 \Omega/\mu\text{m}$ ). The cross sectional area per chain is not obvious given the bundling of many single chains via lateral dipolar chain attraction,<sup>2</sup> which limits the accuracy of resistivity estimates for comparison with other measurements of irreversible nanoparticle wires<sup>7</sup> or rods grown by membrane electrodeposition.<sup>13</sup> In any case, the electrostatic repulsion due to overlapping electrical double

layers plays a vital role in preventing adhesive contacts while providing a path of low resistance that allows such chains to function as “dipolar chain rheostats.”

For the other configurations and transport mechanisms investigated in Figs. 1 and 2, the impedance response was relatively trivial in the case of EO transport but significantly more complicated when EP transport dominates. When colloids were flushed from the electrode gap via EO transport, the impedance response and equivalent circuit were essentially the same as in the unbiased device. For the dominant EP transport at low frequencies, concentrated bands of colloids within the electrode gap produced impedance spectra suggestive of an enhanced capacitive response that is consistent with the parallel electrode/colloid-band arrangement. However, instabilities in the impedance spectra probably require a different measurement configuration to handle large transients in these low frequency measurements. Although the microstructure formed via EP at low applied ac field frequencies needs to be better characterized, its apparent increased capacitance might be exploited as a sort of “electrophoretic varactor.”

In conclusion, our results demonstrate the directed assembly of various colloidal configurations within coplanar microelectrodes via electrokinetic transport, which give rise to unique impedance properties. The success of Eqs. (1)–(3) for interpreting results in the present study provides a basis to explore other devices involving different (1) colloid shapes, sizes, and concentrations, (2) microelectrode geometries and configurations, and (3) material properties including viscosity, dielectric properties, etc. The equivalent circuit models developed in this work reliably distinguish static device impedance properties from resistive, capacitive, and inductive contributions due to colloidal microstructures. The general approach developed in this work, which is to directly connect microstructure, transport, and impedance via quantitative models, should be broadly applicable to the design, control, and optimization of other colloidal based integrated microelectronic/fluidic devices.

The authors acknowledge financial support from DARPA (W911NF-06-1-0050 and FA9550-07-C-0002).

- <sup>1</sup>R. W. O'Brien, D. W. Cannon, and W. N. Rowlands, *J. Colloid Interface Sci.* **173**, 406 (1995).
- <sup>2</sup>T. C. Halsey, *Science* **258**, 761 (1992).
- <sup>3</sup>H. Morgan, M. P. Hughes, and N. G. Green, *Biophys. J.* **77**, 516 (1999).
- <sup>4</sup>R. Krupke, F. Hennrich, H. v. Löhneysen, and M. M. Kappes, *Science* **301**, 344 (2003).
- <sup>5</sup>B. Comiskey, J. D. Albert, H. Yoshizawa, and J. Jacobson, *Nature (London)* **394**, 253 (1998).
- <sup>6</sup>A. Yethiraj and A. v. Blaaderen, *Nature (London)* **421**, 513 (2003).
- <sup>7</sup>K. Hermanson, S. Lumsdon, J. Williams, E. Kaler, and O. Velev, *Science* **294**, 1082 (2001).
- <sup>8</sup>A. Castellanos, A. Ramos, A. Gonzalez, N. G. Green, and H. Morgan, *J. Phys. D* **36**, 2584 (2003).
- <sup>9</sup>R. W. O'Brien, *J. Fluid Mech.* **190**, 71 (1988).
- <sup>10</sup>R. J. Hunter, *Zeta Potential in Colloid Science: Principles and Applications* (Academic, New York, 1981).
- <sup>11</sup>T. B. Jones, *Electromechanics of Particles* (Cambridge University Press, Cambridge, 1995).
- <sup>12</sup>J. Wu, Y. Ben, D. Battigelli, and H.-C. Chang, *Ind. Eng. Chem. Res.* **44**, 2815 (2005).
- <sup>13</sup>P. A. Smith, C. D. Nordquist, T. N. Jackson, T. S. Mayer, B. R. Martin, J. Mbindyo, and T. E. Mallouk, *Appl. Phys. Lett.* **77**, 1399 (2000).